Advances in Science and Technology Research Journal

Advances in Science and Technology Research Journal, 2026, 20(10), 39–53
https://doi.org/10.12913/22998624/224292
ISSN 2299-8624, License CC-BY 4.0

Received: 2026.04.17
Accepted: 2026.08.13
Published: 2026.09.01

Impact of cutting force dynamics on machined surface integrity of maraging steel lattice structures manufactured by selective laser melting

Yevhen Shcherbyna[1], Piotr Niesłony[1*]

[1] Opole University of Technology, ul Mikołajczyka 5, 45-271 Opole, Poland
* Corresponding author's e-mail: p.nieslony@po.edu.pl

ABSTRACT

The presented research aimed to evaluate the machinability and cutting force dynamics of Maraging Steel lattice structures manufactured utilizing SLM technology compared to a monolithic solid reference. Face turning operations were conducted on varying relative densities of 30, 40, and 50% alongside a 100% solid baseline to systematically analyze the effect of a continuous linear decrease in the v_c on the F_c, F_f, and F_p components and the resulting surface integrity. The study reveals that the inherent porosity of the lattice matrix transforms continuous shearing into a harsh intermittent cutting regime inducing severe elasto-plastic yielding and massive relative force fluctuations at low v_c regimes. Furthermore, a critical technological resonance zone was identified at intermediate v_c ranges from 364.60 to 174.47 m/min, where kinetic force spikes primarily dominated by the F_f dynamics directly translated into severe structural tearing and maximum surface roughness. A profound density-resistance paradox was also observed where localized strain-hardening within the topological voids forced the less dense lattice architectures to generate a significantly higher median F_p than the solid material. Ultimately, the experimental findings establish a critical technological guideline for industrial applications, demonstrating that maximizing the v_c effectively overpowers the inherent structural compliance of the lattice, completely suppressing dynamic chatter and guaranteeing superior geometric integrity of the machined struts.

Keywords: face turning, cutting forces, lattice structures, selective laser melting, surface integrity, intermittent cutting, machinability.

INTRODUCTION

Selective laser melting (SLM) is currently one of the key technologies enabling the production of high-performance components for the aerospace and automotive industries [1, 2]. Thanks to the use of metal powders such as Maraging Steel MS1 (1.2709), it is possible to fabricate parts with complex internal geometries, including lattice structures, which offer a superior strength-to-weight ratio [3, 4]. However, faced with the requirements for high dimensional accuracy and surface quality of functional surfaces, manufacturers must subject printed components to post-process machining, usually turning or milling. Regardless of the additive manufacturing precision, the mating surfaces must be machined within strict tolerances to ensure proper assembly and operation [5, 6].

A technology that affects the competitiveness of SLM production is the ability to efficiently machine these porous structures without damaging the delicate internal struts [7, 8]. This process brings major technological challenges. Similar to the drilling of package sheets where individual layers form micro-gaps, the machining of lattice structures is characterized by harsh intermittent cutting conditions [9]. In this type of process, the tool alternates between cutting the solid material of the struts and the voids, which leads to extreme inhomogeneity in the cutting zone. Such extreme kinematic instability inevitably triggers violent force fluctuations and vibrations, severely degrading both insert life and the macroscopic dimensional accuracy of the machined part [7, 10].

Additionally, such stratification of the material results in dynamic impact loads on the cutting edge. An additional complication of conducting this type of process is the frequent use of high-strength steels like MS1, the processing of which affects the wear of the insert much more than standard carbon steels due to pronounced work hardening and abrasive nano-precipitates formed during LPBF [11, 12]. Current literature provides limited data on cutting force dynamics during the face turning of Fluorite topologies, whereas industrial practice frequently reports challenges in maintaining edge integrity [4].

The genesis of this testing is related to the need for high-quality functional surfaces in hybrid manufactured components [13, 14]. Thus, requirements for adequate dimensional and shape tolerance must be met to ensure the industrial applicability of lattice structures [15, 16]. Learning about the impact of cutting speed on the force dynamics in lattice structures is therefore an important piece of engineering knowledge expected by the industry. The presented research aimed to evaluate the machinability of Maraging Steel lattice structures compared to solid material and to define optimal kinematic conditions for minimizing process instability [6, 8].

MATERIALS AND METHODS

Based on information regarding the requirements for high-performance components in the aerospace industry, the research focused on Maraging Steel grade MS1 (1.2709). Four types of disc-shaped specimens with an outer diameter of 84 mm, a thickness of 20 mm, and a central through-hole diameter of 6.2 mm were selected for testing. To evaluate the differences in the processing of lattice architectures compared to solid material, verification tests were performed on a monolithic reference sample manufactured from rolled bar stock alongside three lattice structures with varying relative densities of 30, 40, and 50%. The lattice specimens were manufactured utilizing SLM technology. A detailed characterization of the material used is presented in Table 1 [17].

Table 1. Characteristics of maraging steel MS1 (1.2709)

Chemical composition	Element (weight, %)
Ni	17.0–19.0
Co	8.5–9.5
Mo	4.5–5.2
Ti	0.6–0.8
Al	0.05–0.15
Fe	Balance
Mechanical properties of parts at 20 °C	
Density	8.0–8.1 g/cm^3 (Solid)
Hardness (after aging)	33–37 HRC
Tensile strength for direction XY	1200 ± 100 N/mm^2
Tensile strength for direction Z	1100 ± 150 N/mm^2

The lattice workpiece was manufactured on an EOSINT M280 industrial SLM platform using MS1 metal powder. Specimens featured a fluorite unit cell topology measuring 3 × 3 × 3 mm. Relative density was varied by changing strut thickness while the unit cell size remained constant. Distinct exposure parameters were applied to the core and boundaries to achieve optimal structural integrity. The hatch strategy employed a laser power of 285 W at a scanning speed of 960 mm/s, whereas the contour strategy used 138 W at 300 mm/s. All lattice samples incorporated a circumferential solid wall 2 mm thick, as detailed in Figure 1. A full overview of the tested specimens appears in Table 2.

Face turning tests were performed on an Okuma Genos L200E-M CNC lathe that provides high spindle stability. The cutting force components F_c, F_f, and F_p were measured with a Kistler Type 9129AA multicomponent piezoelectric dynamometer connected to a charge amplifier and recorded through LabVIEW-based software. A Tungaloy ATXOL 2020K25-A tool holder equipped with a Tungaloy 6V-TQMG250604F-TSF T9215 cemented carbide insert served as the cutting tool. This grade features a triple-layer coating consisting of Ti-compound, Al_2O_3, and TiN, which is specifically designed for finishing operations. To minimize the influence of progressive tool wear on the experimental results, each machining test was conducted using a new cutting insert. Additionally, the insert condition was qualitatively evaluated after machining and remained within an acceptable wear range, with no evidence of severe edge degradation. The testing plan relied on face turning under constant kinematic conditions to enable a direct comparison between the solid reference specimen and the lattice structures. For all tested specimens S-100, C-50, C-40, and

Table 2. Configuration of tested specimens

Specimen ID	Structure Type	Topology	Relative Density, %	Manufacturing Method
S-100	Monolithic	Solid	100	Rolled bar stock
C-50	Lattice	Fluorite	50	SLM
C-40	Lattice	Fluorite	40	SLM
C-30	Lattice	Fluorite	30	SLM

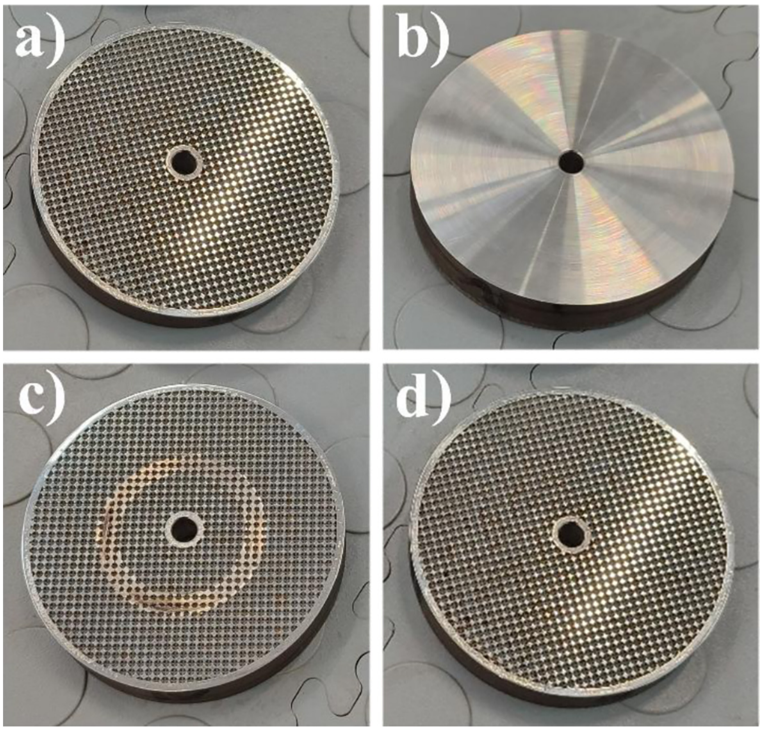

Figure 1. Tested workpieces: a) C-50, b) S-100, c) C-40, d) C-30

C-30 the process parameters remained identical with a spindle speed (*n)* of 2000 rpm, a feed rate (f_n) of 0.1 mm/rev, and a depth of cut (a_p) of 0.1 mm. Tool path progression from the outer periphery at a diameter of 84 mm toward the central hole at a diameter of 6.2 mm produced a continuous linear decrease in cutting speed v_c from a maximum of 527.8 m/min down to 39.0 m/min. This finishing regime permitted evaluation of machinability and force behavior across a wide range of cutting velocities within a single pass.

DATA PROCESSING STRATEGY

To enable the evaluation of cutting force components for different values of relative density, a signal data processing algorithm was implemented, as shown in the flowchart presented in Figure 2. The raw F_c, F_f, and F_p signals generated during the face turning operations were acquired at a constant sampling frequency of 5000 Hz. The experiments were conducted using a single machining pass for each investigated lattice density under constant cutting conditions, while the continuous radial variation of cutting speed provided a highly resolved intra-pass dataset for the analysis of process dynamics. Although the physical machining path spanned from the outer periphery at a radius R of 42 mm to the boundary of the central hole at R of 3.1 mm, the analyzed dataset was trimmed to a unified stable measurement window ranging from R of 39.1 mm to R of 3.8 mm. This preliminary filtering step was strictly necessary to eliminate transient impact phenomena, specifically the tool initial engagement with the 2 mm solid circumferential wall and the instability occurring during the exit phase into the ∅ 6.2 mm through-hole.

Subsequently, a kinematic transformation was applied to provide a technological context for the

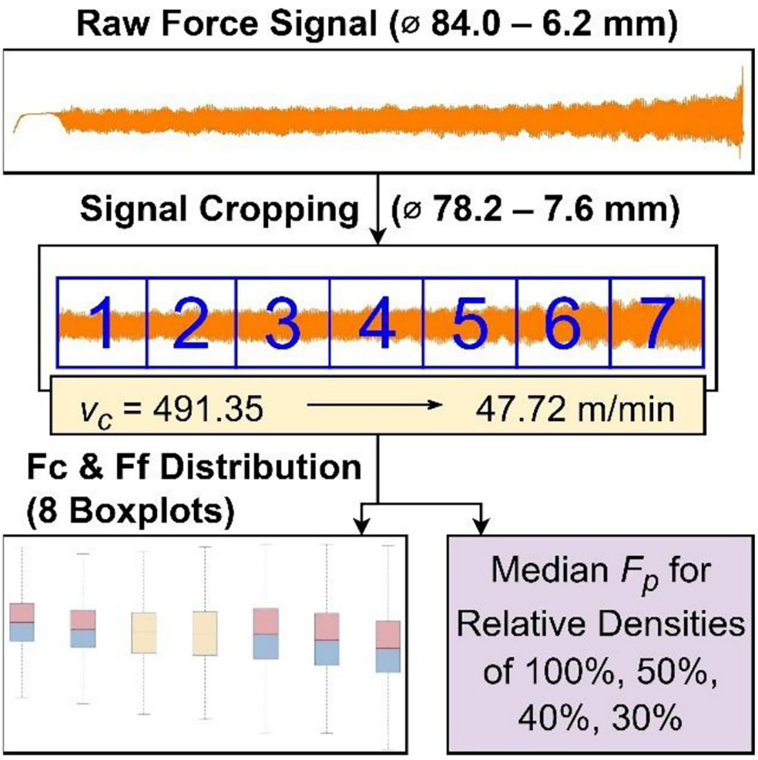

Figure 2. Data processing methodology from raw signal acquisition to comparative correlation analysis

spatial coordinates. The instantaneous v_c measured in m/min was calculated for each measurement point based on the current cutting diameter D, and the constant spindle speed n of 2000 rpm. This transformation established an active evaluated v_c range from 491.35 m/min at the outer boundary down to 47.72 m/min near the center. To accurately capture the dynamic evolution of the intermittent cutting process, the continuous stable data window was further discretized into seven equal radial segments. This segmentation serves as the foundational framework for tracking the process stability as the tool progresses toward the center.

The analytical procedure was then bifurcated based on the physical nature of the individual force components. For the F_c and F_f components, a statistical distribution analysis was utilized. Boxplots were generated for each segment to quantify the process instability and dynamic oscillation severity via the IQR and total whisker spread. Conversely, the F_p was subjected to a trend analysis of its median values to evaluate the variations in axial resistance during the cut. Finally, a comprehensive correlation analysis was performed. The statistical force dynamics from each of the seven zones were directly compared with the resulting surface integrity of the lattice struts. The topological quality was quantified using 3D surface roughness parameters *Ra*, *Rz*, and *Rt*, allowing for a direct evaluation of how kinematic conditions and force dispersion dictate the physical material removal mechanisms in SLM lattice structures.

RESULTS AND DISCUSSION

Statistical analysis of the F_c and F_f dynamics

The evaluation of the cutting force dynamics must fundamentally begin with the monolithic S-100 reference sample to establish a thermodynamic and kinematic baseline. As expected in conventional continuous face turning, the solid 100% material exhibits a highly stable material removal mechanism governed by continuous plastic deformation and shearing. This stability is quantitatively evidenced by a narrowly constrained IQR approximating 2 to 11.5 N across all cutting speeds for both the F_c and F_f components as illustrated in Figure 3 and Figure 4.

When normalized against the median force to evaluate relative process volatility, this solid baseline demonstrates exceptional dynamic stability, with the interquartile boundaries deviating by only 0.9% to 4.4% from the median throughout

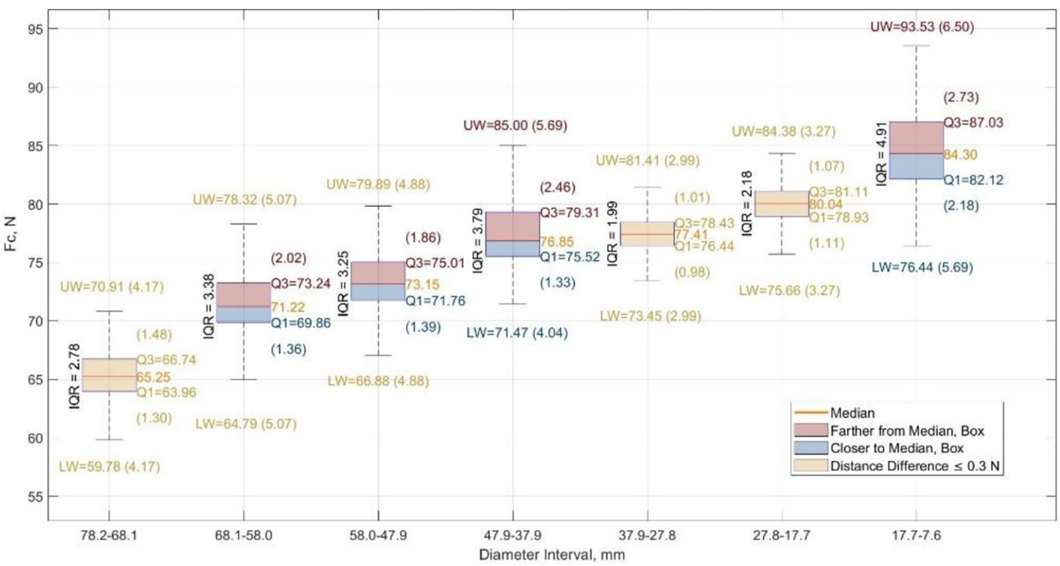

Figure 3. Statistical distribution of the F_c across radial intervals for S-100

the entire kinematic spectrum. Furthermore, as the v_c increases from the center towards the periphery, the median force smoothly declines, confirming the dominant role of classical thermal softening in the primary shear zone.

However, the transition to processing SLM lattice architectures including C-50, C-40 and C-30 introduces a severe disruption to this equilibrium functioning as a topological shock to the machining system. The inherent porosity of the Fluorite unit cell transforms the continuous shear process into an aggressive intermittent cutting regime. This fundamental shift in the physical interaction is distinctly captured by the extreme expansion of the statistical distribution limits, specifically the whisker spread detailed in Figure 5 through Figure 10. The severity of this topological shock is most apparent when evaluating the relative force dispersion. For instance, while the absolute nominal load decreases when transitioning to the critically sparse C-30 structure, its relative process instability exponentially magnifies. At the lowest cutting velocities, the interquartile boundaries for the 30% lattice deviate by a pronounced reduction +93.4% and -83.7% from the median F_c compared to the negligible ±3.2% deviation observed in the solid reference.

In the lattice structures, the UW values spike dramatically and frequently exceed the nominal median force by a factor of two or more. These

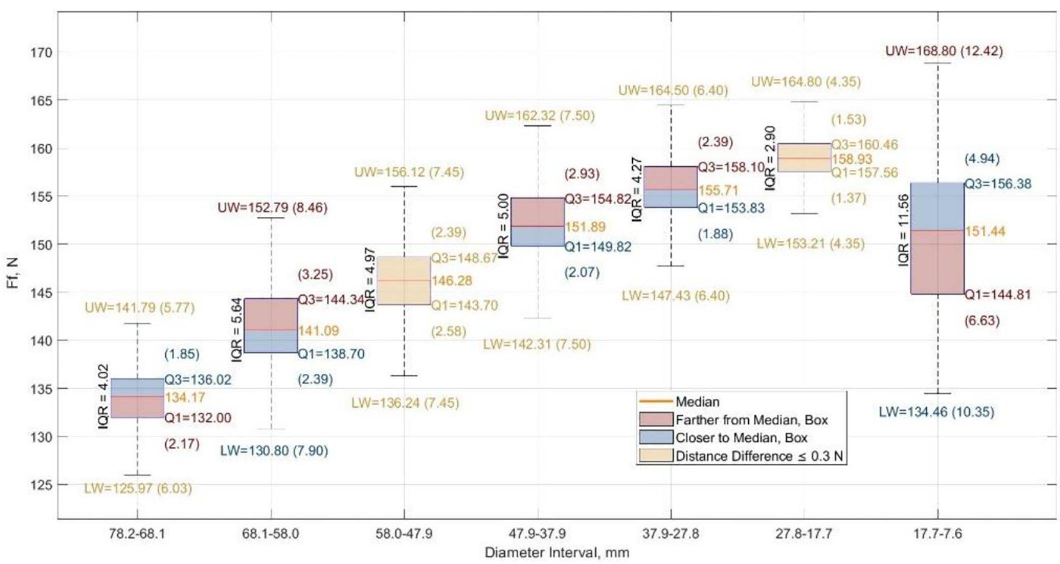

Figure 4. Statistical distribution of the F_f across radial intervals for S-100

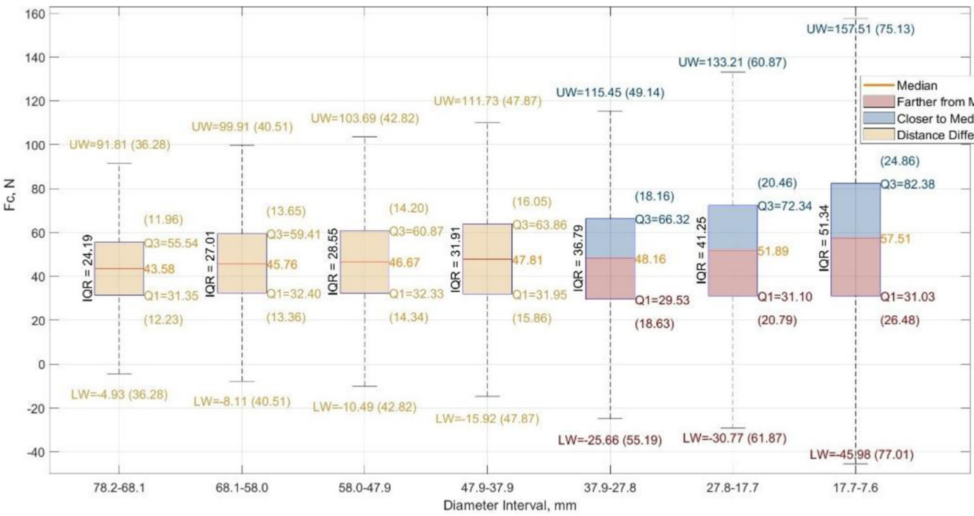

Figure 5. Statistical distribution of the F_c across radial intervals for C-50

extreme positive peaks represent the rigid, high-energy impact loads generated at the exact millisecond the cutting edge engages the unyielding solid wall of a lattice strut. Conversely, a critical physical anomaly characterizing the lattice machining is observed in the LW behavior. While the solid material maintains strictly positive LW values that closely track the median, the lattice topologies generate deep negative LW metrics often plunging tens of Newtons below zero as demonstrated in Figure 7 and Figure 9. This deep negative force is a direct physical manifestation of severe elastic rebound and mechanical relaxation within the tool-holder system. As the insert abruptly exits a metallic strut and plunges into a topological void, the elastic deflection accumulated during the impact phase is violently released, causing the tool to pull back and oscillate. Consequently, the macro-dynamics of machining lattice topologies cannot be treated merely as a scaled-down version of solid material cutting proportional to the density, as it is a fundamentally distinct process dominated by cyclic impact-induced structural deflection and sudden elastic recovery.

Despite the severe intermittent conditions inherent to the C-50 and C-40 lattice structures, a distinct kinetic stabilization is observed in the F_c as the v_c increases. Moving from the low-speed central zone towards the high-speed periphery, the statistical dispersion of the F_c undergoes a critical contraction. This is quantitatively demonstrated by the relative process volatility which normalizes the IQR limits against the median cutting load to evaluate true structural instability. In the C-50 specimen detailed in Figure 5,

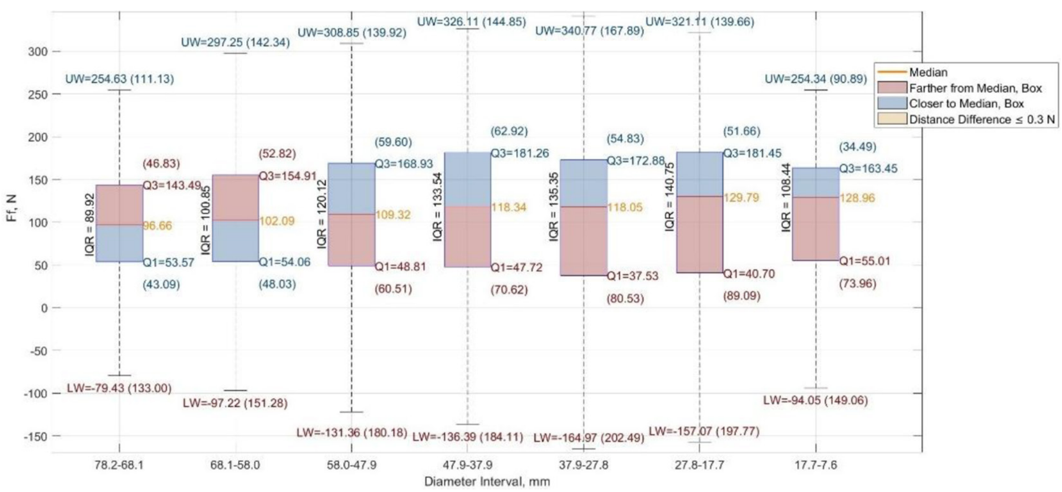

Figure 6. Statistical distribution of the F_f across radial intervals for C-50

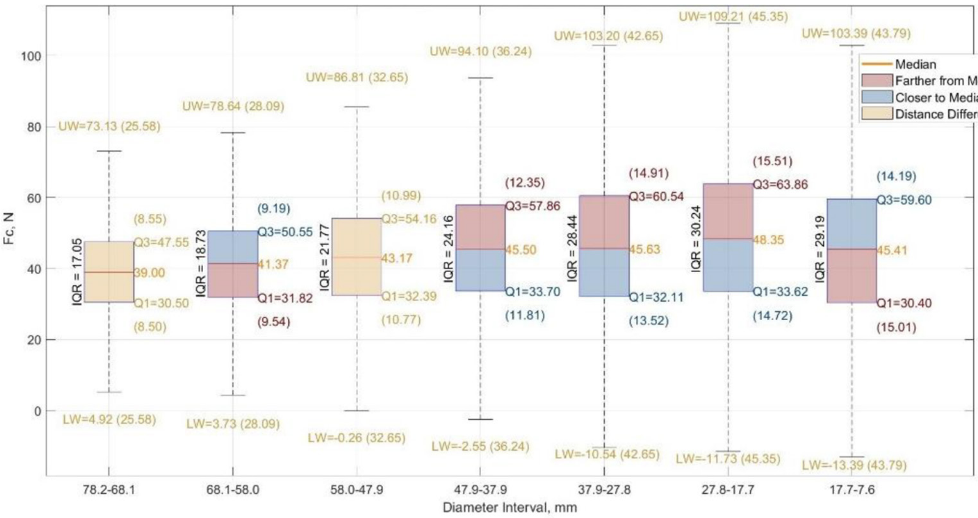

Figure 7. Statistical distribution of the F_c across radial intervals for C-40

the relative dispersion of the quartiles shrinks dramatically from +43.2% and -46.0% at the lowest velocities down to +27.4% and -28.1% at the highest speeds. Furthermore, the cross-structural comparative analysis reveals a highly non-linear density-stability relationship where the C-40 structure presented in Figure 7 unexpectedly emerges as a technological sweet spot exhibiting significantly tighter relative stability limits that contract from roughly ±32% down to ±21.8% compared to the denser C-50 topology. This indicates that the thicker struts in the 50% fill generate excessively rigid impact loads known as a hammering effect, whereas the 40% density provides a more optimal balance of structural compliance and shearing resistance.

This progressive stabilization reflects not only reduced mechanical vibrations but a genuine shift in the material removal mechanism governed by the strain rate effect. At lower cutting speeds the interaction time between the cutting edge and individual lattice struts increases substantially. Owing to the limited bending stiffness of the thin struts, the tool drives the material into an elasto-plastic bending and squeezing regime known as ploughing prior to actual chip separation. This behaviour produces wide force fluctuations and highly erratic loads.

In contrast, when v_c exceeds 400 m/min the strain rate rises sharply. Tool velocity then surpasses the propagation speed of gross plastic deformation inside the strut, which promotes

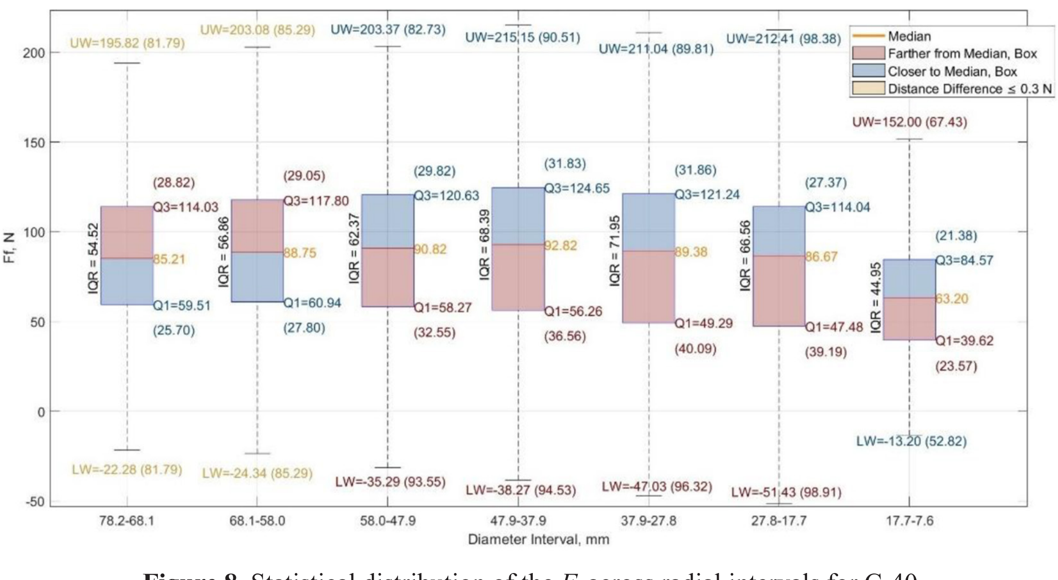

Figure 8. Statistical distribution of the F_f across radial intervals for C-40

adiabatic localized shearing. Under these conditions the lattice struts are severed cleanly before significant deflection or bending can occur. As a result, the relative amplitude of dynamic force oscillations drops abruptly to the topological minimum. High-speed cutting therefore constitutes an essential technological requirement for SLM lattice topologies. It effectively compensates for their structural compliance and enforces stable shearing instead of erratic ploughing.

While the C-50 and C-40 structures generally adhere to the principle of thermal softening by exhibiting a gradual decrease in the median F_c at higher velocities, the C-30 topology presents a profound physical anomaly. As observed in the statistical distribution for the 30 percent relative density specimen presented in Figure 9, the median F_c undergoes a complete kinematic inversion. At the lowest cutting speeds near the center of the workpiece, the median force is surprisingly minimized and records values as low as 17.45 N, whereas at the highest peripheral speeds, it nearly doubles to reach 33.07 N.

This inverse relationship contradicts classical machining theory yet aligns fully with the extreme loss of topological stiffness. In the C-30 structure the individual lattice struts are critically thin and exhibit minimal cross-sectional inertia. At low cutting speeds these fragile struts cannot provide adequate resistance to the advancing cutting edge. As a result, the tool predominantly deflects and bends the struts rather than initiating proper chip formation. The material undergoes severe elasto-plastic yielding, which produces a deceptively low median force because the lattice matrix is pushed aside instead of being cleanly sheared. However, this low force is accompanied by massive relative IQR fluctuations indicating constant structural flutter and erratic tearing rather than stable machining. Quantitatively, the relative dispersion analysis exposes the absolute severity of this structural collapse: at the lowest v_c dropping below 111 m/min, the interquartile boundaries for the C-30 structure violently deviate by +93.4% and -83.7% from the median F_c. This extreme relative percentage confirms that stable cutting is practically nonexistent, replaced entirely by cyclic tearing and unconstrained vibration.

Conversely, as the v_c escalates to the maximum range, the rapid tool engagement denies the struts the necessary time to elastically deflect. The high strain rate effectively overpowers the lack of structural stiffness by forcing the material directly into an adiabatic shearing mechanism. While the actual shearing and separation of the strut demand a higher nominal energy input that consequently raises the median F_c, this mechanism simultaneously enforces kinematic stability. This stiffness paradox conclusively demonstrates that below a critical topological density threshold, classical cutting laws collapse and process stability becomes entirely reliant on achieving strain rates high enough to overcome the inherent structural compliance of the lattice matrix.

In contrast to F_c, the F_f component exhibits pronounced sensitivity to the intermittent microgeometry of the lattice matrix along the tool path. The monolithic S-100 specimen maintains a consistently narrow force dispersion across the entire kinematic range, as shown in Figure 4. In

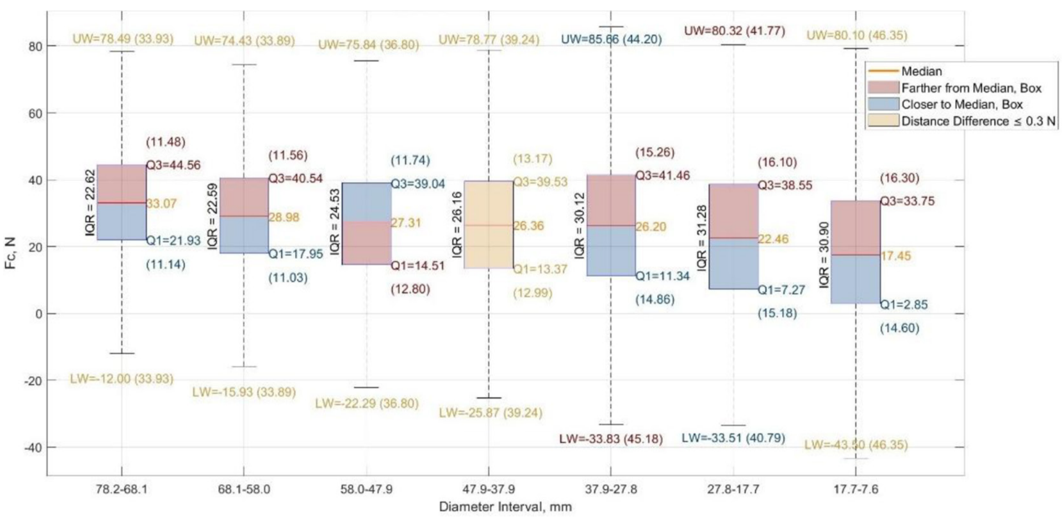

Figure 9. Statistical distribution of the F_c across radial intervals for C-30

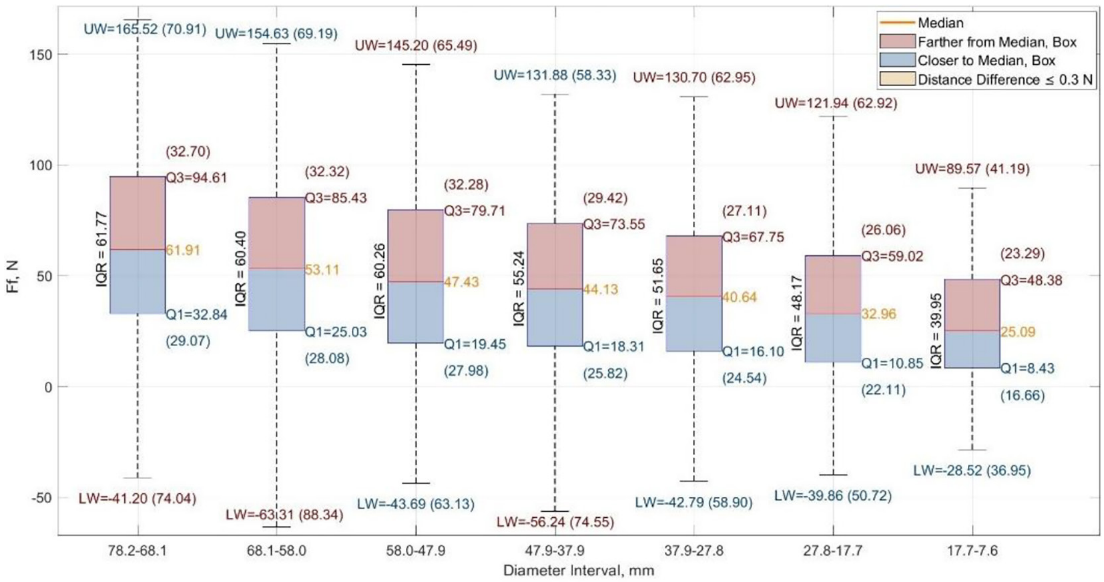

Figure 10. Statistical distribution of the F_f across radial intervals for C-30

comparison, the lattice topologies C-50, C-40, and C-30 display highly non-linear volatility profiles, as illustrated in Figure 6, Figure 8, and Figure 10. The statistical boxplots reveal that the maximum instability, characterized by the widest IQR and the most extreme whisker spread, does not occur at the lowest v_c but rather manifests as a distinct volatility hump in the intermediate velocity range corresponding to the v_c interval between 364 m/min and 174 m/min.

This mid-speed instability is explicitly validated by the relative dispersion metrics. For instance, in the denser C-50 topology, the Q1 drops by 44.6% at the maximum peripheral v_c and 57.4% at the lowest central v_c. However, within the intermediate velocity zone, this downward deviation drastically amplifies and plummets to 68.6% relative to the median. This suggests the presence of a technological resonance zone. Within this specific kinematic window, the structural passing frequency, defined as the rate at which the cutting edge engages the solid struts and disengages into the topological voids, likely aligns with the natural frequency of the tool-workpiece system elastic deflection. Alternatively, this velocity range corresponds to thermomechanical conditions highly conducive to unstable built-up edge formation and cyclic tear-off, further aggravating the cutting resistance. As a result, the tool is subjected to amplified axial oscillations violently pulling and pushing the insert, which is quantitatively reflected in the massive peak-to-valley distance between the UW and LW.

It is only by accelerating beyond this resonant barrier into the high-speed regime where the v_c exceeds 400 m/min that the F_f relative dispersion reliably compresses below the 50 percent threshold, allowing the process to regain kinetic stability. Consequently, from an industrial application perspective, a critical technological guideline for the machining of SLM lattice architectures is established: an intermediate v_c provokes exponential increases in relative dynamic chatter and must be strictly avoided. Therefore, the application of high cutting-speed kinematics is critical for reducing feed-direction vibrations and ensuring the geometric integrity of the machined struts.

Evaluation of axial resistance and the F_p anomaly

While the F_c and F_f generally exhibit a predictable reduction in nominal load with decreasing material density, the F_p demonstrates a profound physical anomaly. The comparative analysis of the median F_p trends summarized in Figure 11 reveals a severe density-resistance paradox that fundamentally contradicts conventional continuous machining principles. As established by the monolithic S-100 baseline, a continuous face turning process generates a highly stable F_p trajectory maintaining a relatively consistent axial resistance that ranges exactly from a maximum of 22.75 N to a minimum of 17.26 N across the entire kinematic spectrum. Furthermore, the relative dispersion analysis confirms this process stability with the interquartile boundaries for the solid reference deviating by a tightly constrained +9.4% to -8.3% from the median. However, in the high to intermediate v_c ranges corresponding to the diameter intervals from 78.2 mm down to 27.8 mm, the C-50 and C-40 lattice topologies consistently generate a significantly higher median axial resistance than the 100 percent solid material reaching peak values of 26.22 N and 28.43 N respectively as presented in Figure 11.

This counterintuitive inversion arises from localized densification and strain-hardening induced by the intermittent cutting of lattice architectures. During continuous turning of the solid material, F_p is governed exclusively by the steady-state mechanics of the primary and secondary shear zones. In contrast, machining the lattice matrix involves repetitive impacts of the insert against individual struts, which induce severe elasto-plastic axial compression prior to actual material separation. Furthermore, due to the intermittent tool-workpiece engagement, the generated micro-chips and plastically deformed strut edges are frequently forced and packed into the adjacent topological voids rather than being effectively evacuated. This localized accumulation creates a compacted and highly work-hardened cushion of material directly ahead of the cutting edge. Consequently, the tool must constantly overcome this artificially densified structural barrier resulting in a substantial amplification of the F_p component despite the reduction in the macroscopic material volume. The severity of this interaction is quantitatively reflected in the relative process volatility, where engagement with the hardened topological accumulation layer induces significant axial vibrations, resulting in relative dispersion limits for the C-50 structure reaching +293.2% and −283.0% at the lowest cutting speeds. Such an extreme fluctuation confirms that the tool is subjected to violent and unconstrained axial bouncing rather than steady-state engagement.

Conversely, as the process enters the low-speed regime toward the workpiece centre, a pronounced secondary effect appears most clearly in the C-30 topology. While the C-50 and C-40 structures exhibit a relatively gradual decline in axial resistance, the specimen with 30% relative density demonstrates a pronounced reduction in the F_p component, as illustrated by the blue trajectory in Figure 11. At the high-speed peripheral zone corresponding to the diameter interval from 78.2 to 68.1 mm, the median F_p for the C-30 structure registers at a substantial 26.51 N. However, as the v_c decreases radially inward, this absolute resistance plummets linearly and reaches a mere 9.48 N in the lowest v_c interval from 17.7 to 7.6 mm. This steep gradient is governed by the strain-rate stiffening effect combined with a critical loss of topological rigidity. At a high v_c, the elevated strain rate forces the structurally fragile 30 percent lattice to shear before it can undergo gross axial deflection, thereby generating significant passive resistance and somewhat constraining the relative force dispersion by recording a +71.6% and -67.1% deviation from the median.

However, as the tool advances toward the centre and v_c decreases, the engagement time

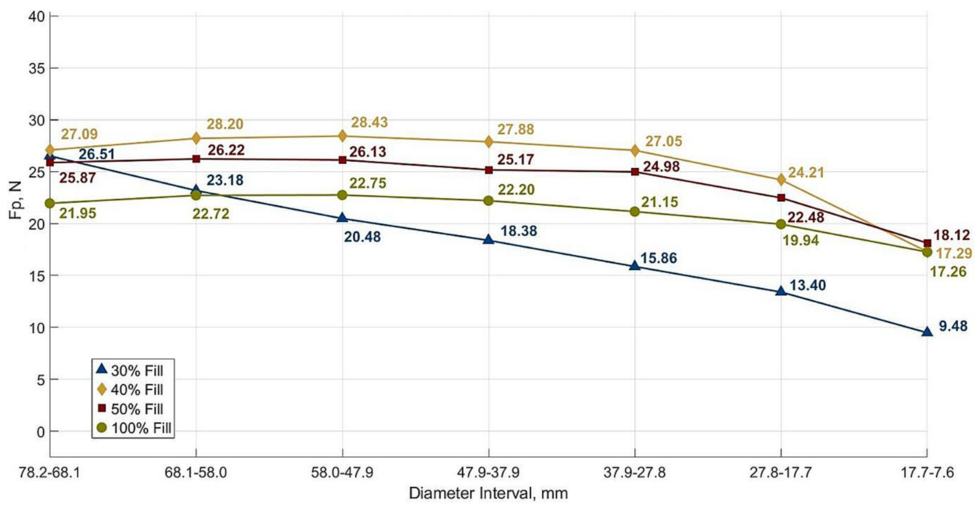

Figure 11. Comparison of median F_p trends across varying relative densities as a function of the radial tool position

between the insert and individual struts increases markedly. The exceptionally thin struts of the C-30 topology lack sufficient bending stiffness to resist the advancing cutting edge. Rather than being cleanly sheared, the material elasto-plastically deflects and yields axially, essentially bending away from the advancing tool. This inability of the material to support the cutting mechanism explains the drastic drop in the F_p to 9.48 N. Crucially, the relative dispersion analysis exposes the perilous nature of this low-force regime where, as the absolute force minimizes, the relative axial volatility undergoes an explosive expansion driving the interquartile boundaries to an extreme +176.5% and -158.5% from the median.

This profound variation in the F_p across the radial tool path has critical implications for dimensional stability. Because the F_p component directly dictates the degree of tool deflection, the severe macroscopic radial drop of F_p from 26.51 N down to 9.48 N compounded by microscopic relative vibrations exceeding 176% will inevitably induce highly erratic and variable dynamic spring-back of the tool-holder system. Consequently, the variable axial yielding of the lattice matrix makes it highly susceptible to macro-geometric shape deviations fundamentally manifesting as flatness errors or conicity on the machined face of the lattice component.

Surface integrity and correlation with the physical material removal mechanisms

To correlate cutting force behaviour with surface topological quality, the machined surfaces were examined using an optical profilometer. The acquired topographic data exported in.plux format were processed with MountainsMap Expert 10 software. The data extraction procedure specifically adapted for the intermittent micro-geometry of lattice architectures is detailed in the flowchart in Figure 12. This pipeline includes radial segmentation, TLSPL surface leveling, critical threshold determination to isolate struts from voids, and extraction of 30 profiles per zone. The approach separates the data into Top Profiles representing the upper envelope and Mean Profiles used to quantify local micro-defects.

In the adopted methodology, the Top Profiles represent the upper geometric envelope of the lattice struts and are primarily used to evaluate the macroscopic surface integrity of the machined structure. In contrast, the Mean Profiles are averaged representations extracted from multiple local measurements and are intended to quantify localized micro-defects and surface irregularities generated by the intermittent cutting mechanism. Consequently, the upper-envelope parameters describe the extreme topographical variations

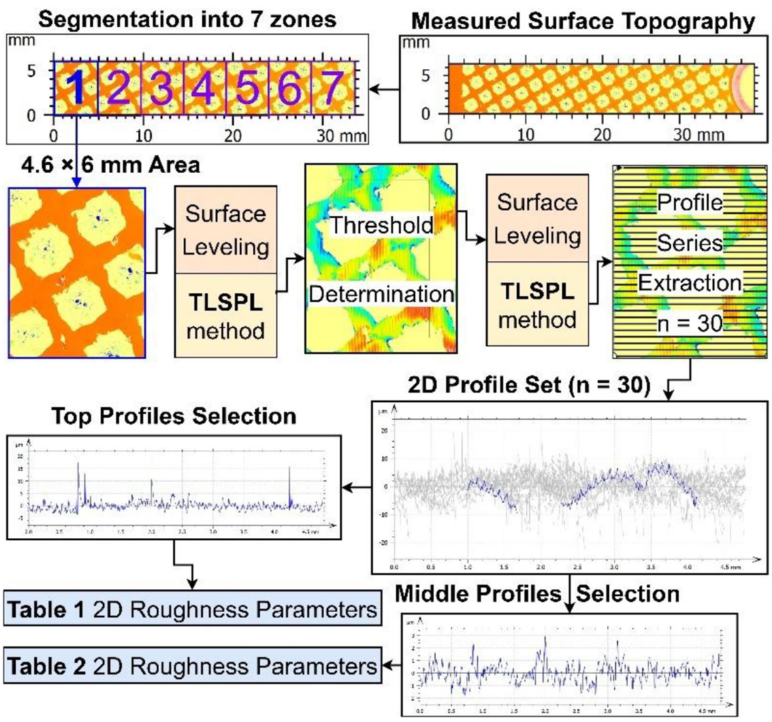

Figure 12. Topographic data extraction and profile segmentation flowchart

of the lattice surface, whereas the conventional roughness parameters provide a generalized characterization of the local surface finish.

In contrast, data extraction for the monolithic S-100 reference was considerably simplified owing to its continuous topology. The solid surface was segmented into seven kinematic zones and leveled using the standard TLSPL procedure. Threshold masking and multi-profile statistical averaging were omitted. Instead, baseline roughness parameters were obtained by extracting a single representative profile line per zone. These yielded *Ra* values from 0.6 to 0.9 µm, *Rz* from 3.5 to 5.3 µm, and *Rt* from 4.5 to 9.7 µm as illustrated in Figure 13, thereby providing a strict kinematic reference for the continuous shearing mechanism.

The comparative analysis of the roughness parameters reveals a direct physical correlation between kinematic instability and topological degradation. Specifically, Zone 5 corresponding to intermediate v_c exhibits peak roughness values for the lattice architectures as detailed for the *Rz* parameter in Table 3 and visually represented in Figure 14. While the monolithic S-100 specimen maintains a highly stable *Rz* magnitude of approximately 5.3 µm in this region, the C-40 structure demonstrates extreme deterioration. The *Rz* upper envelope for C-40 spikes to 26.3 µm alongside an *Rt* mean profile reaching 23.0 µm as documented in Table 4 and illustrated in Figure 15. This severe topological damage directly mirrors the cutting force dynamics. As established in the force analysis, zones 5 and 6 generate the maximum statistical dispersion for the F_c within the C-40 structure. The amplified IQR and extreme whisker spread in these intermediate v_c ranges translate physically into violent tool vibrations. These vibrations literally tear the lattice struts and create the massive micro-defects captured by the profilometer.

Within this intermediate v_c range, the C-50 lattice structure constitutes a notable exception by preserving a remarkably stable topological profile across the entire v_c spectrum. As explicitly shown in Table 3, the *Rz* upper envelope for the 50% relative density specimen varies only between 11.8 µm and 9.2 µm. Furthermore, its *Rt* mean profile remains tightly bounded between 4.5 µm and 11.5 µm as confirmed by Table 4 and the graphical trends in Figure 15. This consistent surface topography contrasts sharply with the erratic micro-geometry of the lower-density architectures. The underlying reason is the increased bending stiffness provided by the thicker lattice struts at higher relative density. Although the C-50

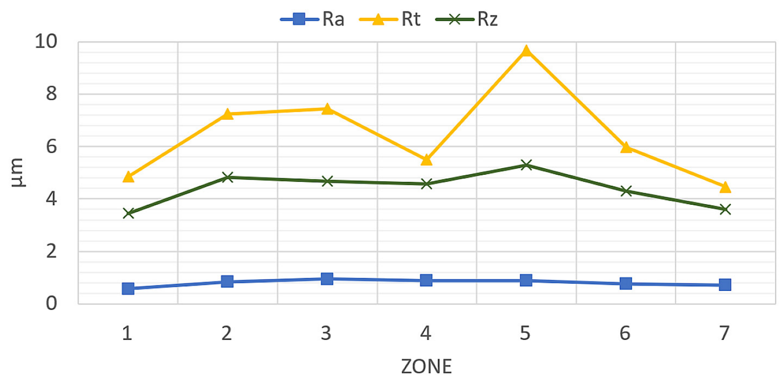

Figure 13. Surface roughness parameters *Ra*, *Rz*, and *Rt* for S-100

Table 3. Upper envelope maximum profile height *Rz* across kinematic zones

v_c, m/min	Zone	C-50 (µm)	C-40 (µm)	C-30 (µm)
491.35–427.97	1	11.1	14.5	8.2
427.97–364.60	2	11.3	10.2	17.1
364.60–301.22	3	11.8	7.9	24.3
301.22–237.85	4	10.4	20.3	16.0
237.85–174.47	5	10.1	26.3	19.7
174.47–111.10	6	10.8	4.9	12.2
111.10–47.72	7	9.2	11.8	8.0

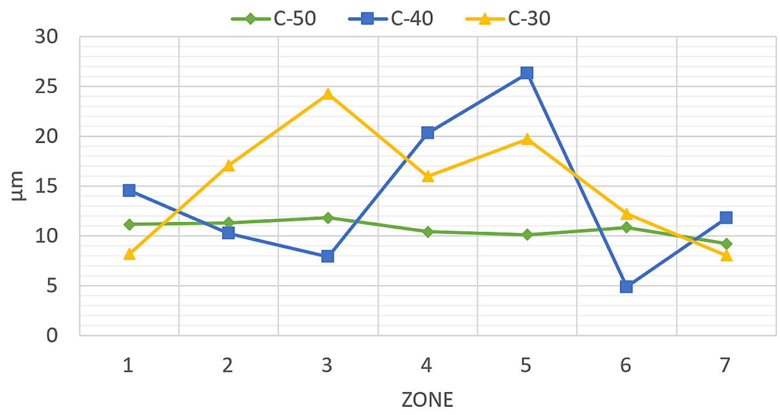

Figure 14. Upper envelope maximum profile height *Rz* for the tested lattice structures

Table 4. Mean profile total height *Rt* across kinematic zones

v_c, m/min	Zone	C-50 (µm)	C-40 (µm)	C-30 (µm)
491.35–427.97	1	10.8	12.4	3.8
427.97–364.60	2	9.1	4.0	5.9
364.60–301.22	3	4.5	3.4	8.7
301.22–237.85	4	11.5	17.7	6.0
237.85–174.47	5	9.5	23.0	7.2
174.47–111.10	6	5.0	3.0	5.9
111.10–47.72	7	5.6	14.5	4.0

topology generates significant localized F_p peaks, the struts retain sufficient mechanical rigidity to withstand these dynamic loads without substantial fracture or excessive plastic deformation. This resistance to micro-tearing enables the C-50 structure to closely approach the consistent surface finish observed on the monolithic S-100 reference.

At the highest v_c in Zone 1, a universal improvement in surface quality is observed across all tested densities. This regime yields the lowest roughness values where the *Rz* upper envelope reaches 11.1 µm for C-50, 14.5 µm for C-40, and 8.2 µm for C-30 as comprehensively summarized in Table 3 and Figure 14. These reduced roughness metrics directly reflect the kinetic stabilization seen in the cutting force boxplots. The narrowed force dispersion and minimized elastic rebound at peak v_c promote stable shearing. The tool cleanly severs the struts before significant plastic deformation can develop, thereby suppressing the vibrational tearing typical of lower v_c zones and delivering superior surface integrity.

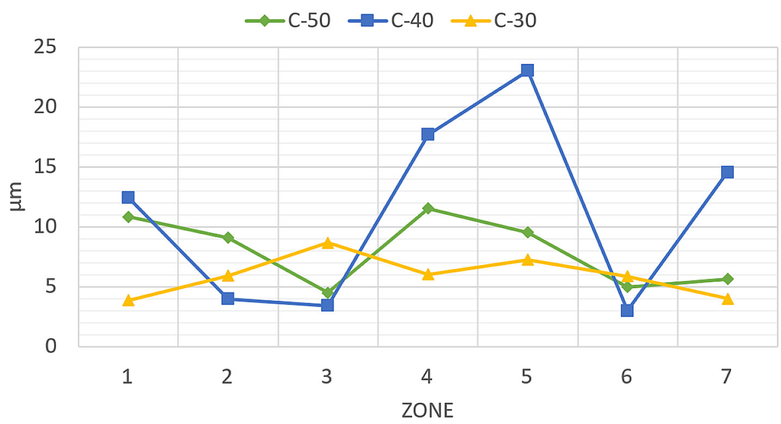

Figure 15. Mean profile total height *Rt* for the tested lattice structures

CONCLUSIONS

Face turning operations provided a highly effective kinematic framework for evaluating a broad cutting speed (v_c) spectrum ranging continuously from 491.35 to 47.72 m/min. This approach facilitated a direct comparative analysis between SLM Maraging Steel lattice structures with varying relative densities of 30, 40, and 50% and a monolithic rolled baseline. The experimental results revealed the profound impact of cutting velocity on force dynamics, demonstrating that lattice architectures generate exponentially greater kinematic instability than steady-state continuous machining of solid material. Quantifying this extreme intermittent volatility required the development of a specialized signal-processing algorithm for cutting forces. Subsequently, to establish a robust physical correlation between these dynamic mechanical loads and the resulting surface integrity, a tailored topographic data-extraction methodology was engineered for the complex microgeometry of the lattice struts. The application of these newly integrated analytical frameworks yields the following primary conclusions:

A highly specialized analytical methodology was successfully developed and implemented for the precise evaluation of surface quality in SLM lattice structures. This tailored topological approach effectively isolates the intermittent lattice struts from deep structural voids, enabling accurate quantification of local micro-defects.

The kinematic evaluation demonstrated that superior surface quality characterized by minimal roughness metrics is achievable at the extreme boundaries of the tested v_c spectrum. Specifically, the lowest topological roughness was reliably obtained at the highest v_c, ranging from 491.35 to 427.97 m/min, and in the lowest v_c regime, from 111.10 to 47.72 m/min.

A critical technological resonance zone was identified in the intermediate v_c ranges. Extreme surface roughness, indicating severe process instability and significant material damage during transition phases, was generated exclusively within the intermediate v_c window ranging from 364.60 to 174.47 m/min.

A direct physical correlation was established between the surface roughness severity and the F_f dynamics during face turning. The F_f component dominated the generation of peak mechanical loads, with kinetic force spikes directly translating into large surface roughness peaks. This dynamic degradation mechanism is most clearly evident in the extreme topological deterioration observed in the 40% relative density specimen.

The relative material density profoundly dictates the overall machinability and structural resilience of the manufactured component. The highest tested lattice density of 50% exhibited the most stable and minimized roughness indicators across the entire v_c spectrum. This confirms that a higher material fill provides the essential bending stiffness needed to resist intermittent impact loads and stabilize the material-removal mechanism.

REFERENCES

1. Khan N., Riccio A. A systematic review of design for additive manufacturing of aerospace lattice structures: Current trends and future directions. Prog. Aerosp. Sci. 2024; 149: 101021. https://doi.org/10.1016/j.paerosci.2024.101021
2. Gao B., Zhao H., Peng L., Sun Z. A review of research progress in selective laser melting (SLM). Micromachines 2022; 14(1): 57. https://doi.org/10.3390/mi14010057
3. Li Y., Jiang D., Zhao R., Wang X., Wang L., Zhang L.-C. High mechanical performance of lattice structures fabricated by additive manufacturing. Metals 2024; 14(10): 1165. https://doi.org/10.3390/met14101165
4. Maconachie T., Leary M., Lozanovski B., Zhang X., Qian M., Faruque O., Brandt M. SLM lattice structures: Properties, performance, applications and challenges. Mater. Des. 2019; 183: 108137. https://doi.org/10.1016/j.matdes.2019.108137
5. Dias J.M., da Silva F.S.C.P., Gasik M., Miranda M.G.M., Bartolomeu F.J.F. Unveiling additively manufactured cellular structures in hip implants: A comprehensive review. Int. J. Adv. Manuf. Technol. 2024; 130(9–10): 4073–4122. https://doi.org/10.1007/s00170-023-12769-0
6. Freitas B., Richhariya V., Silva M., Vaz A., Lopes S.F., Carvalho Ó. A review of hybrid manufacturing: Integrating subtractive and additive manufacturing. Materials 2025; 18(18): 4249. https://doi.org/10.3390/ma18184249
7. Javed A., Khan A.M., Zhao G., Jamil M., Schoop J., Wang C., et al. The defect-postprocessing-lifecycle nexus: a critical review of interdependencies in metal additive-subtractive manufacturing. Int. J. Adv. Manuf. Technol. 2025; 141(1–2): 31–76. https://doi.org/10.1007/s00170-025-16600-w
8. Smith S., Schmitz T., Feldhausen T., Sealy M. Hybrid metal additive/subtractive machine tools and

applications. CIRP Annals 2024; 73(2): 615–638. https://doi.org/10.1016/j.cirp.2024.05.002

9. Wieczorek Ł., Józwik J., Niesłony P., Moj K. The influence of cutting parameters and tool wear on the quality of holes in package sheets used in heat exchangers. Adv. Sci. Technol. Res. J. 2025; 19(4): 156–170. https://doi.org/10.12913/22998624/195585
10. Yang Y., Yan S., Qu S., Yi M., Chen Z., Zhou T., et al. Microstructure of titanium alloy in additive/subtractive hybrid manufacturing: A review. J. Alloys Compd. 2025; 1014: 178769. https://doi.org/10.1016/j.jallcom.2025.178769
11. Halilovic S., Wild N., Orsolic M., Huskic A. Influence of process parameters and wall thicknesses on the properties of tool steel 1.2709 (X3NiCoMoTi18-9-5) processed by selective laser melting. Procedia Comput. Sci. 2025; 253: 853–862. https://doi.org/10.1016/j.procs.2025.01.147
12. Raghuraman V., Kumar T.S. The impact of different heat treatments on the surface characteristics, residual stresses, and tensile strength of maraging steel 1.2709 samples produced by LPBF. Results Eng. 2025; 26: 105509. https://doi.org/10.1016/j.rineng.2025.105509
13. Dennison M.S., S K.J., M A.M. Life cycle assessment in hybrid additive-subtractive manufacturing of titanium medical implants-a step towards sustainability. Int. J. Adv. Manuf. Technol. 2025; 141(1–2): 77–108. https://doi.org/10.1007/s00170-025-16765-4
14. Du W., Li X., Zhang J., Chen C., Zhu S. Review of hybrid additive-subtractive manufacturing of stainless steel for repair applications. Addit. Manuf. Front. 2026; 5(1): 200290. https://doi.org/10.1016/j.amf.2025.200290
15. Wang Y., Zhao Q., Li G., Li X. Mechanical performance of additive manufactured tpms lattice structures based on topology optimization. Comput. Model. Eng. Sci. 2025; 144(1): 763–789. https://doi.org/10.32604/cmes.2025.067363
16. Yang J., Liu H., Cai G., Jin H. Additive Manufacturing and influencing factors of lattice structures: A review. Materials 2025; 18(7): 1397. https://doi.org/10.3390/ma18071397
17. EOS Maraging Steel MS1. Material Data Sheet. 2023. https://www.eos.info/metal-solutions/metal-materials/data-sheets/mds-eos-maragingsteel-ms1 (Accessed: 12.10.2023).